Spectroscopic Investigation of the Molecular Vibrations of 1,4-Dihydronaphthalene in Its Ground and Excited Electronic States

Mohamed Z. M. Rishard,[†] Martin Wagner,[†] Jaebum Choo,[‡] and Jaan Laane*,[†]

Department of Chemistry, Texas A&M University, College Station, Texas 77843-3255, and Department of Chemistry, Hanyang University, 425-791 Ansan, Korea

Received: March 24, 2009; Revised Manuscript Received: May 7, 2009

A comprehensive spectroscopic study of 1,4-dihydronaphthalene (14DHN) has been carried out for its ground and $S_1(\pi,\pi^*)$ electronic states using infrared, Raman, ultraviolet, and laser-induced fluorescence (LIF) spectroscopic techniques. The experimental work was complemented by ab initio and DFT calculations. For the ground state excellent agreement between observed and calculated values was attained. For the $S_1(\pi,\pi^*)$ excited state 19 of the vibrational modes were clearly determined and excited vibronic levels for a number of these were also identified. A detailed energy map for the low-frequency modes in both electronic states was established. 14DHN is very floppy in its S_0 ground state but less so in its excited state. The floppiness relaxes C_{2v} selection rules for the S_0 state.

Introduction

Recently we reported[1] the laser-induced fluorescence (LIF) and ultraviolet (UV) absorption spectra associated with the ring-puckering vibration of 1,4-dihydronaphthalene (14DHN). From these the ring-puckering potential energy function was determined for both the S_0 and $S_1(\pi,\pi^*)$ states and this showed the molecule to be planar in both electronic states. However, in the $S_1(\pi,\pi^*)$ state the molecule was found to be much more rigid. In the present paper we report a comprehensive study of the vibrations of 14DHN in both its S_0 and $S_1(\pi,\pi^*)$ states and compare the results to theoretical calculations. These results provide a deeper insight into the energetics of the 14DHN molecule.

Experimental Section

The sample of 14DHN was purchased from TCI America and purified by trap-to-trap distillation. However, the sample still contained a few percent of 1,2-dihydronaphthalene, which we had previously studied[2] and for which the spectra were thoroughly analyzed.

The experimental procedures for the acquisition of the LIF spectra have been previously described.[2−10] The UV absorption spectra were recorded using a Bomem DA8.02 Fourier transform spectrometer and the LIF spectra were obtained using an apparatus based on a Continuum Sunlite OPO laser system. The Raman spectra of 14DHN were acquired on an SA Jobin-Yvon U-1000 spectrometer equipped with a liquid-nitrogen-cooled CCD (charge couple device) detector. Raman scattering was achieved using a Coherent Radiation Innova 20 argon ion laser with excitation at 514.5 nm or a Verdi-10 at 532 nm. The liquid-phase spectra were recorded at room temperature with lasing power of 0.2−0.6 W. Vapor-phase Raman spectra were collected in the previously described vapor Raman cell[11] at a temperature of 300 °C. A laser power of 5 W was used for the vapor studies. The mid-infrared spectra of a thin capillary film of the pure sample between two KBr disks were collected on the Bruker Vertex 70 FT-IR spectrometer. Typically 256 scans with a resolution of 1 cm^{-1} were recorded. Boxcar apodization was utilized.

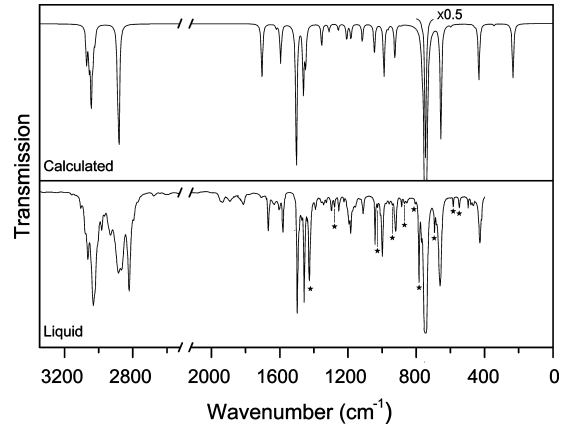

Figure 1. Liquid-phase infrared spectra of 14DHN compared to its calculated DFT spectrum.

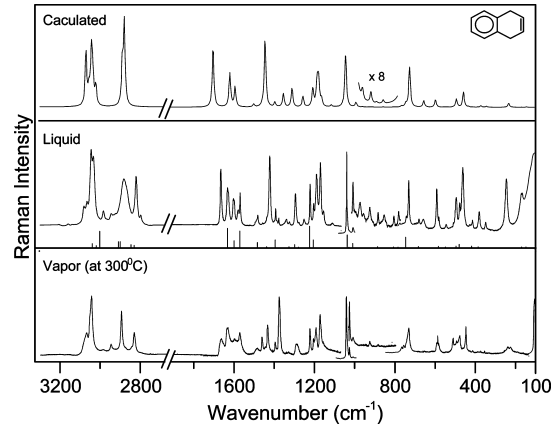

Figure 2. Liquid- and vapor-phase Raman spectra of 14DHN compared to its calculated DFT spectrum. The liquid-phase Raman spectrum of 12DHN is also shown for comparison as vertical bars.

[†] Texas A&M University.
[‡] Hanyang University.

10.1021/jp902672x CCC: $40.75
Published on Web 06/10/2009

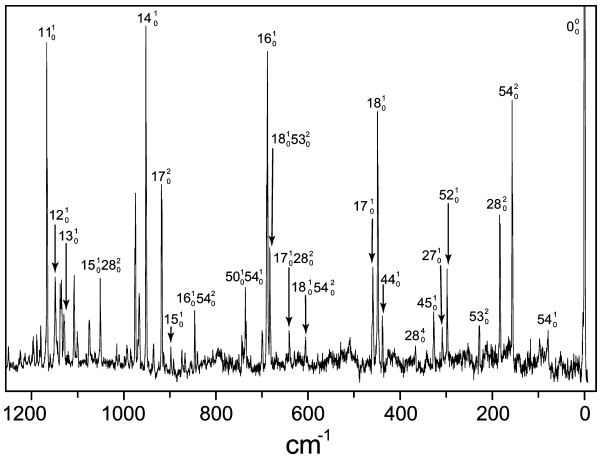

Figure 3. FES spectrum of 14DHN with some assignments.

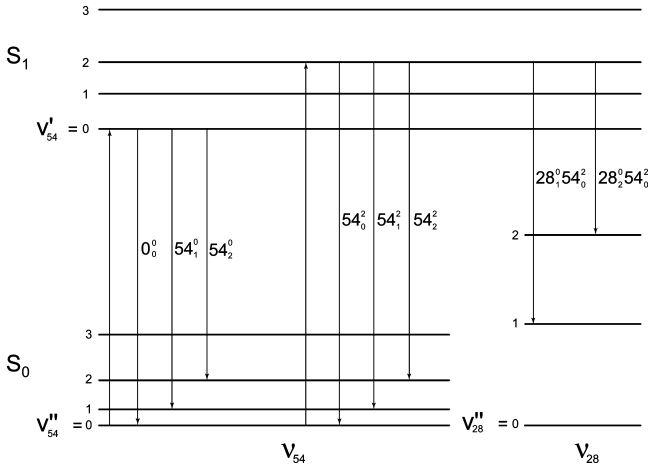

Figure 4. Labeling scheme for SVLF spectra acquired by different excitations.

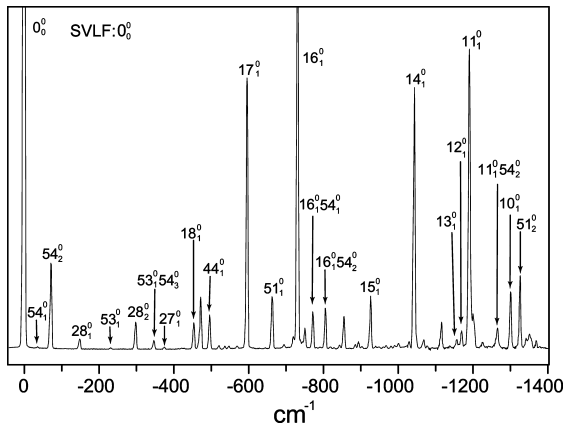

Figure 5. SVLF spectra of 14DHN from 0_0^0 excitation.

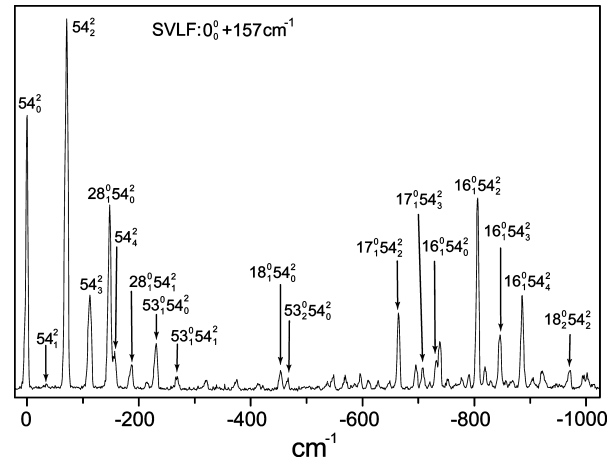

Figure 6. SVLF spectra of 14DHN from 54_0^2 excitation.

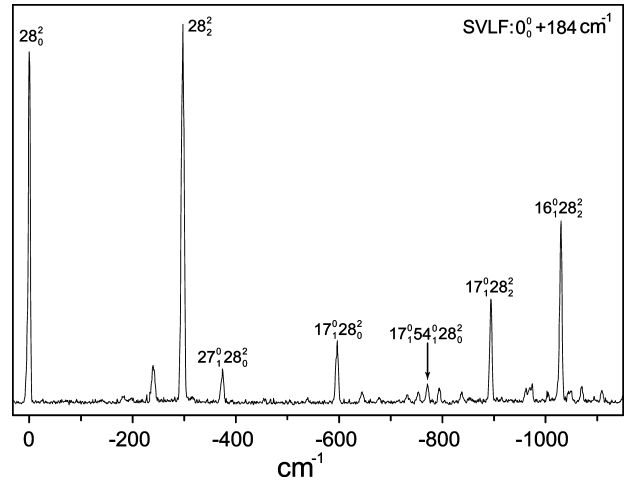

Figure 7. SVLF spectra of 14DHN from 53_0^2 excitation.

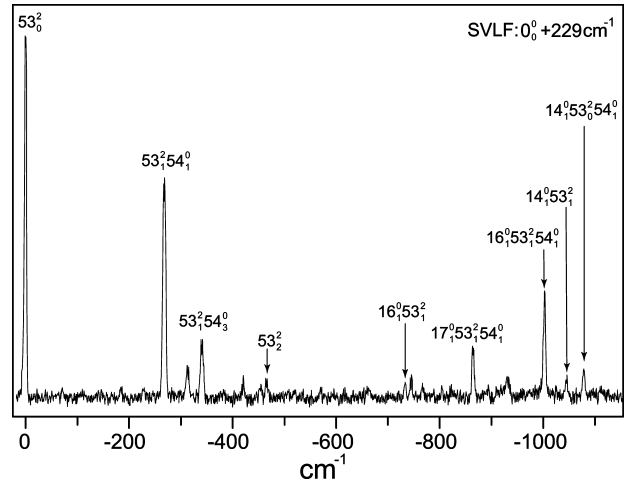

Figure 8. SVLF spectra of 14DHN from 53_0^2 excitation.

Computations

All of the computations were carried out using the Gaussian 03 quantum mechanical package.[12] The vibrational frequencies, infrared and Raman intensities, and depolarization ratios of 14DHN in its S_0 state were calculated using the B3LYP/6-311++G(d,p) level of theory. Calculated frequencies were scaled by a factor of 0.964 for values over 1800 cm^{-1} and a factor of 0.985 for those below 1800 cm^{-1}, as from previous work.[13−16] The $S_1(\pi,\pi^*)$ state calculations were done at the CIS/6-311++G(d,p) level of theory for the planar C_{2v} structure. The scaling factor was 0.895, which had also been used for 12DHN. The CIS (configuration interaction-singles) is an inexpensive ab initio method which can be applied for excited electronic state calculations. It is comparable to the Hartree−Fock method used for the ground state and therefore does not take the electron correlation effects fully into account. More rigorous computational methods such as time-dependent density functional theory and CIS(D) (or CIS with

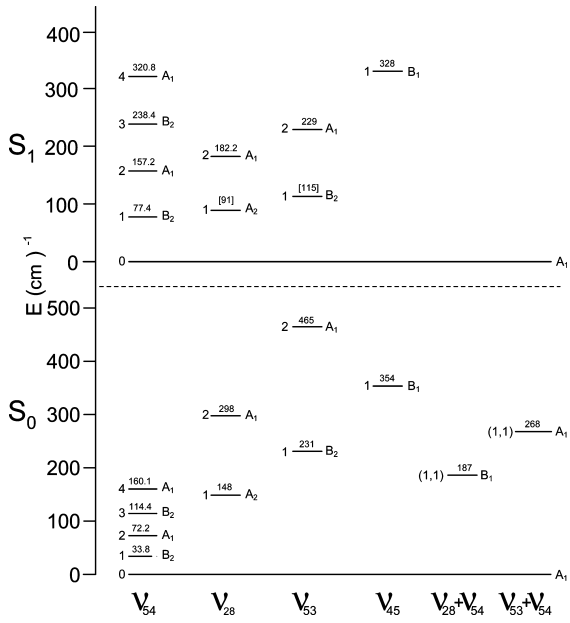

Figure 9. Energy level diagram of 14DHN for the low-frequency vibrational levels.

second-order correction) were also carried out to determine the excited state structure and vibrational frequencies. However, all of these methods failed to calculate the minimum energy structure. Nevertheless, the CIS calculations have provided fairly reasonable results, and this will be noted later.

Although this work reports the frequencies calculated only for the planar structure (C_{2v}) of 14DHN, computations were also performed for C_s (bent) and C_1 (structure with no symmetry) point groups as well. The calculated values for the C_s and C_1 structures were very similar to those of the C_{2v} structure and therefore are not presented here. The approximate descriptions of the vibrational normal modes were determined by the GaussView 3.0 molecular visualization program.[17]

Results and Discussion

Infrared and Raman Spectra. Our previous study of 14DHN showed that this molecule has a planar structure with C_{2v} symmetry in both the ground and $S_1(\pi,\pi^*)$ electronic states.[1] Therefore the distribution of the 54 vibrational modes of 14DHN can be expressed as

$$18A_1 + 10A_2 + 17B_1 + 9B_2$$

The A_1, B_1, and B_2 modes are infrared active while all are Raman active. The 18 A_1 modes should be Raman polarized. Figures 1 and 2 compare the infrared and Raman spectra of 14DHN to the computed scaled spectra using the DFT-B3LYP/6-311++G(d,p) level of calculation. Table 1 lists the values of the experimental and calculated vibrational frequencies and their relative intensities according to the symmetry species. Most of the bands predicted by the theoretical computations agree very well with the experimental spectra, but a few extra bands were observed in the actual spectra. A close analysis revealed that these peaks belong to those of 1,2-dihydronaphthalene (12DHN), an isomer of 14DHN, whose vibrational spectra have previously been assigned.[2] The most intense peaks of 12DHN are at 782 and 1224 cm^{-1} in the infrared and Raman spectra, respectively, and can be clearly observed in the spectra illustrated here also. The frequencies and intensities of the other impurity peaks also agree very well with those of 12DHN. This information is useful as no information about the impurities present in the commercial 14DHN had been provided by the manufacturer or by anyone who used the same source of sample before.[18] Figure 1 marks the most intense 12DHN impurity bands present in the liquid infrared spectra with asterisks. Figure 2 shows a line spectrum of the impurity derived from the original liquid Raman spectrum[2] of 12DHN. After the 12DHN peaks were eliminated, the agreement between the calculated and experimental data for 14DHN is very good. The experimental depolarization ratios (ρ values) of the liquid Raman spectra are also listed in Table 1 together with their relative intensities. Most of the vibrational modes which are totally symmetric with A_1 symmetry have very low ρ values (i.e., polarized) while the other modes which are nontotally symmetric (with A_2, B_1, and B_2 symmetries) have high ρ values, close to the theoretical value of 0.75. A few of these, however, have lower ρ values, and this may be caused by the overlap with polarized bands or by the nonrigidity of the molecule as it flops back and forth by more than 20° of puckering. The observed differences occur since the polarization ratios of the Raman system were not calibrated at different wavenumbers. The calculated frequencies of the $S_1(\pi,\pi^*)$ electronic states using the CIS/6-311++G(d,p) level of theory are also listed in Table 1 along with some of the experimental values from the fluorescence excitation spectra (FES). The comparison of calculated and observed frequencies of the excited state will be discussed below.

Fluorescence Excitation Spectra (FES). We previously reported the FES of 14DHN related to the ring-bending vibration. Here we present a more comprehensive analysis of the FES data. Figure 3 shows the FES spectrum of 14DHN along with a number of the assignments. Table 2 lists the wavenumbers of the bands and the corresponding values observed in the ultraviolet absorption spectra (UV) together with the calculated frequencies from the CIS/6-311++G(d,p) ab initio calculation. Most of the observed bands listed in Table 2 correspond to the vibrations of A_1 symmetry, and these agree very well with the calculated values. The validity of these assignments is further supported by the observation of bands corresponding to the combinations of these fundamental A_1 modes with the overtones of the lowest three vibrational modes such as $18_0^1 54_0^2$, $15_0^1 53_0^2$, and $14_0^1 28_0^2$ which are also totally symmetric. Only a few bands with symmetry species other than A_1 were observed, and these are relatively weak compared to the totally symmetric vibrations. Table 2 also lists some of the "cold" UV absorption bands corresponding to the FES bands. UV bands can also originate from higher vibrational levels in S_0, and these will be discussed later.

Single Vibronic Level Fluorescence (SVLF) Spectra. SVLF or dispersed fluorescence spectra can also be used to determine the vibrational levels of the S_0 ground state. The advantage of utilizing SVLF is that it can also elucidate the higher vibrational quantum states ($v = 2, 3, 4, ...$). Overtone bands can sometimes also be observed in infrared and Raman spectra, but their intensities are generally too weak. Figure 4 shows the labeling scheme for SVLF transitions along with several examples of observed transitions.

TABLE 1: Vibrational Assignment (in cm^{-1}) of 1,4-Dihydronaphthalene[a]

				Raman			calculated	
C_{2v} symmetry	no.	approx description	IR liquid	liquid[c]	vapor[d]	FES[b]	S_0[e]	$S_1(\pi,\pi^*)$[f]
A_1	1	benzene C−H stretch	3077 sh	3080 (9, 0.2)	3067 (37)		3071 (108, 81)	3015
	2	=C−H stretch		3045 (33, 0.1)	3042 (90)		3044 (223, 79)	2994
	3	benzene C−H stretch		(3045)	(3042)		3037 (4, 44)	2973
	4	CH_2 stretch		(2882)	2893 (70)		2880 (8, 124)	2785
	5	C=C stretch	1667 ms	1668 (18, 0.1)	1663 (9)		1705 (39, 109)	1674
	6	benzene C−C stretch	1581 ms	1572 (2, 0.2)	1571 (3)		1595 (28, 37)	1625
	7	benzene C−H ip wag	1497 vs	1497 sh			1504 (100, 5)	1518
	8	CH_2 deform		1425 (19, 0.3)	1433 (12)		1447 (0.03, 124)	1417
	9	CH_2 wag	1342 w	1342 (1, 0.5)		1400 ms	1356 (14, 13)	1396
	10	benzene C−C stretch	1297 m	1298 (7, 0.1)	1288 (5)	1337 ms	1313 (5, 34)	1336
	11	benzene C−C stretch				1167 vs	1188 (2, 46)	1153
	12	=C−H wag	1173 sh	1172 (14, 0.2)	1172 (16)	1149 m	1181 (0.4, 49)	1142
	13	benzene C−H ip wag	1156 w	1157 (3, 0.5)	1156 (4)	1130 m	1166 (0.04, 13)	1129
	14	benzene C−C stretch	1041 s	1042 (100, 0.1)	1041 (100)	951 vs	1047 (21, 100)	960
	15	sat. ring C−C stretch				873 w	919 (0.5, 8)	878
	16	sat. ring C−C stretch	(746)	734 (45, 0.1)	730 (38)	689 vs	728 (2, 75)	669
	17	ring angle bend		596 (5, 0.1)	586 (11)	459 ms	599 (2, 13)	517
	18	ring angle bend			446 (15)	449 s	460 (2, 28)	434
A_2	19	CH_2 stretch		(2882)	(2893)		2890 (0, 58)	2789
	20	CH_2 twist					1213 (0, 1)	1163
	21	=C−H out-of-plane wag	976 sh	976 (1, D)			995 (0, 8)	996
	22	benzene C−H oop wag					974 (0, 0.05)	904
	23	CH_2 rock		958 (0.1, D)			961 (0, 1)	813
A_2	24	benzene C−H oop wag	855 w	856 (1, D)			859 (0, 0.2)	630
	25	benzene ring twist		703 (vw, ?)			708 (0, 0.003)	447
	26	benzene ring twist		513 (1, ?)	510 (7)		499 (0, 0.001)	360
	27	C=C twist		384 (2, D)	373 (1)	310 mw	373 (0, 3)	288
	28	ring twist at the bridge				(92)	146 (0, 0.3)	70
B_1	29	benzene C−H stretch	3064 ms	3065 (11, 0.3)	3073 sh		3056 (105, 22)	3004
	30	benzene C−H stretch	3031 vs	3034 (30, 0.2)	(3042)		3034 (76, 1)	2988
	31	=C−H stretch	(3031)	(3034)	(3042)		3022 (43, 28)	2950
	32	CH_2 stretch	2884 ms	2882 (18, 0.2)	2874 sh		2881 (328, 3)	2779
	33	benzene C−C stretch	1603 m	1605 (10, D)			1621 (3, 63)	1415
	34	benzene C−C stretch	1456 s	1462 (1, 0.3)	1460 (7)		1463 (46, 1)	1406
	35	CH_2 deform	1426 s				1449 (26, 2)	1375
	36	=C−H in-plane wag	1389 mw	1381 (3, 0.2)	1375 (27)		1398 (0.004, 9)	1369
	37	CH_2 wag	1355 w				1356 (1, 12)	1320
	38	benzene C−H ip wag	1254 m	1255 (2, D)			1258 (4, 19)	1145
	39	sat. ring C−C stretch	1184 ms				1184 (9, 0.5)	1112
	40	benzene C−H ip wag	1111 ms	1112 (1, D)			1118 (12, 4)	1036
	41	sat. ring C−C stretch	998 s			967 ms	990 (37, 1)	947
	42	ring angle bend	885 m			867 w	891 (1, 0.1)	851
	43	ring angle bend	769 m	762 (1, 0.1)	765 (7)		769 (11, 1)	707
	44	ring angle bend	496 m	498 (2, D)	493 (3)	439 m	495 (0.2, 15)	424
	45	ring angle bend		351 (1, D)	354 (1)	328 m	346 (1, 2)	312
B_2	46	CH_2 stretch	(2884)	(2882)	(2874)		2889 (151, 2)	2788
	47	CH_2 wag	1193 mw	1192 (10, 0.1)	1192 (10)		1209 (11, 32)	1163
	48	benzene C−H oop wag	959 w				967 (2, 0.06)	910
	49	CH_2 rock	920 ms		925 (2)		927 (24, 0.002)	711
	50	benzene C−H oop wag	746 vs	746 (2, 0.2)			747 (448, 5)	653
	51	=C−H out-of-plane wag	660 vs	661 (1, 0.D)	661 (1)		657 (78, 12)	593
	52	benzene ring oop vibration	427 ms	430 (0.1, D)		298 ms	435 (40, 1)	261
	53	sat. ring flapping		248 (6, D)	231 (5)	(115)	235 (38, 7)	90
	54	sat. ring puckering				79 vw	36 (4, 1)	72

[a] Key: s, strong; m, medium; w, weak; v, very; sh, shoulder; ip, in-phase; oop, out-of-phase. [b] The values in the parentheses are approximate expected values. [c] The relative Raman intensities and the depolarization ratios are shown in parentheses. D = depolarized (0.75) within experimental error. [d] The relative Raman intensities are shown in parentheses. [e] Calculated using B3LYP/6-311++G(d,p) level of theory. The relative infrared and Raman intensities are shown in the parentheses. The original calculated values were scaled by a factor of 0.985 for frequencies below 2000 cm^{-1} and by a factor of 0.964 cm^{-1} for those above 2000 cm^{-1}. [f] Calculated using CIS/6-311++G(d,p) level of theory. The scaling factor used was 0.895.

The SVLF spectrum of 14DHN originating from the 0_0^0 excitation is illustrated in Figure 5, and Table 3 lists the wavenumber values along with those from the 54_0^2 (0_0^0 + 157 cm^{-1}), 28_0^2 (0_0^0 + 184 cm^{-1}), and 53_0^2 (0_0^0 + 229 cm^{-1}) excitations, The most intense bands can be seen to be from the totally symmetric transitions such as $A_1 \rightarrow A_1$, but a number of the nontotally symmetric transitions can also be seen. Two A_1 vibrational modes (ν_{15} and ν_{11}) which were

TABLE 2: FES Spectrum of 14DHN Compared to Some Selected UV Bands (cm^{-1})

FES	UV	assignment (sym.)	calculated[a]	inferred[b]
79 vw	77.2 m	54_0^1 (B_2)	72	
157 s	157.2 ms	54_0^2 (A_1)		
184 ms	182.2 w	28_0^2 (A_1)		
229 m	228.8 w	53_0^2 (A_1)		
298 ms	299.2 w	52_0^2 (B_2)?	261	
310 mw		27_0^1 (A_2)?	288	
328 m	327.1 vw	45_0^1 (B_1)	312	
367 w	366.7 w	28_0^4 (A_1)		
439 m	438.5 w	44_0^1 (B_1)	424	
449 s	448.4 m	18_0^1 (A_1)	434	
459 ms	461.0 mw	17_0^1 (A_1)	517	
459 ms	461.0 mw	53_0^4 (A_1)		2×229
606 w	606.9 vw	$18_0^1 54_0^2$ (A_1)		$449 + 157$
630 vw	630.7 w	$18_0^1 28_0^2$ (A_1)		$449 + 184$
640 w	639.5 vw	$17_0^1 28_0^2$ (A_1)		$459 + 184$
682 ms	681.8 ms	$18_0^1 53_0^2$ (A_1)		$449 + 229$
689 vs	687.6 m	16_0^1 (A_1)	669	
699 m	698.5 vw	?		
735 m	732.4 ms	$50_0^1 54_0^1$ (A_1)		$(653) + 79$
846 m	846.0 w	$16_0^1 54_0^2$ (A_1)		$689 + 157$
867 w	866.7 mw	42_0^1 (B_1)	851	
873 w	874.4 vw	15_0^1 (A_1)	878	
873 w	874.4 vw	$16_0^1 28_0^2$ (A_1)		$689 + 184$
897 mw	895.5 w	18_0^2 (A_1)		2×449
918 s	917.4 ms	17_0^2 (A_1)		2×459
918 s	917.4 ms	$16_0^1 53_0^2$ (A_1)		$689 + 229$
935 m	935.5 mw	?		
951 vs	951.2 vs	14_0^1 (A_1)	960	
967 ms	967.1 mw	41_0^1 (B_1)	947	
975 s	975.1 mw	?		
1051 ms	1050.9 mw	$15_0^1 28_0^2$ (A_1)		$873 + 184$
1075 m	1074.3 mw	$17_0^2 54_0^2$ (A_1)		$918 + 157$
1100 w	1100.5 vw	$15_0^1 53_0^2$ (A_1)		$873 + 229$
1108 m	1108.4 ms	$14_0^1 54_0^2$ (A_1)		$951 + 157$
1130 m	1131.9 mw	13_0^1 (A_1)	1129	
1135 m	1134.0 w	$14_0^1 28_0^2$ (A_1)		$951 + 184$
1149 m	1147.3 m	12_0^1 (A_1)	1142	
1167 vs	1166.2 ms	11_0^1 (A_1)	1153	
1180 w	1179.8 w	$14_0^1 53_0^2$ (A_1)		$951 + 229$
1323 m	1322.2 w	$11_0^1 54_0^2$ (A_1)		$1167 + 157$
1337 ms	1335.7 mw	10_0^1 (A_1)	1336	
1341 ms	1340.7 w	18_0^3 (A_1)		3×449
1350 m	1350.0 vw	$11_0^1 28_0^2$ (A_1)		$1167 + 184$
1355 m	1355.0 vw	$13_0^1 53_0^2$ (A_1)		$1130 + 229$
1373 m		17_0^3 (A_1)		3×459
1376 mw		16_0^2 (A_1)		2×689
1395 vw		$11_0^1 53_0^2$ (A_1)		$1167 + 229$
1400 ms		9_0^1 (A_1)	1396	

[a] Calculated using CIS/6-311++G(d,p) level of theory. [b] Inferred from the already assigned fundamental values or from the calculated values.

not detected in the infrared or Raman spectra were observed in SVLF and their frequencies match almost perfectly well with the calculated frequencies. Notably, some nontotally symmetric transitions were also observed including one at -148 cm^{-1} which is assigned to 28_1^0. This originates from a forbidden $A_1 \rightarrow A_2$ transition but matches the calculated value of 148 cm^{-1} for this twisting motion. The floppy nature of the 14DHN ring and the high degree of anharmonicity of its low-frequency modes apparently account for the observations of such "forbidden" transitions. Interestingly, the 28_0^1 excitation transition, which is expected near 92 cm^{-1}, is not clearly observed. Since the ring is much stiffer in the S_1 state, this transition may be more restricted by the selection rules of the planar C_{2v} structure. This is even clearer when the FES and 0_0^0 SVLF spectra are compared where the latter shows many nontotally symmetric transitions while the former has very few.

Figure 6 shows the SVLF spectrum recorded from the 54_0^2 ($0_0^0 + 157$ cm^{-1}) excitation. Some of the assignments were previously discussed,[1] but more detail is presented here. These data enabled us to determine many levels of the ring puckering mode (ν_{54}) of the S_0 state and were utilized for determining the potential energy function of 14DHN in the S_0 state.

Figures 7 and 8 depict two other SVLF spectra originating from the 28_0^2 ($0_0^0 + 184$ cm^{-1}) and 53_0^2 ($0_0^0 + 229$ cm^{-1}) excitations, respectively. The very intense band at -298 cm^{-1} in Figure 7 is clearly the 28_2^2 transition which confirms the assignment of 184 cm^{-1} to 28_0^2 in the FES spectra. The absence of a 28_1^2 peak at -148 cm^{-1} is a little surprising as this was observed in the other SVLF spectra. The 53_0^2 excitation also gives rise to a weak SVLF band at -465 cm^{-1}, and this corresponds to 53_2^2. The very strong peak at -268 cm^{-1} clearly belongs to the $53_2^2 54_1^0$ transition, a combination level of ring-puckering and ring-flapping modes. Table 3 lists the frequency values and their assignments of four of the SVLF spectra discussed here. Nine of the 18 A_1 vibrational modes (ν_{10} to ν_{18}) were clearly observed for the S_0 state, and their frequencies match extremely well with those reported in Table 1. In addition, some combinations of these modes with ν_{54} also have been observed confirming the accuracy of the assignments. Although the majority of the transitions are totally symmetric, there are a few exceptions. Some of these have considerable intensities (e.g., ν_{44} and ν_{51}). This supports our argument that the floppiness of the molecule relaxes the C_{2v} selection rules, and hence some forbidden transitions can be observed.

Ultraviolet Absorption Spectra. The assignment of the UV data is rather more complicated than the assignment of all the other spectra discussed. Unlike FES, the UV spectra were recorded at ambient temperature or higher. Therefore, higher vibrational levels from which transitions can originate can also be significantly populated and many "hot bands" can be observed. Table 4 lists a number of these observed bands and these typically provide more accurate wavenumber values (0.2 cm^{-1}) than the FES or SVLF values (1 cm^{-1}). Together with the FES and SVLF spectra, a very clear picture of the energies of the vibrational levels of the molecule can be elucidated which can give a wealth of information on the molecule.

Figure 9 shows the energy diagram for the vibrational energy levels of 14DHN in its S_0 and S_1 states determined from the data in Tables 1−4 for the FES, UV, SVLF, infrared, and Raman spectra. While accurate values for many of the levels in the excited state were determined, in a few cases approximate values were estimated, and these are shown in parentheses.

The infrared and Raman spectra showed the presence of 12DHN as an impurity in the 14DHN sample. This was again confirmed by the UV spectra which showed a series of very low intense bands whose origin is at 34093 cm^{-1}. This value perfectly agrees with the previously reported value for the 0_0^0 band of 12DHN.[2] Since the band origins for 12DHN and 14DHN (with 0_0^0 is at 36788.6 cm^{-1}) are about 2700 cm^{-1} apart, the two spectra are readily distinguishable.

Conclusions

Spectroscopic analysis of 14DHN using FES, SVLF, UV, infrared, and Raman techniques allowed us to determine the energies of many vibrational and vibronic levels of this molecule in its ground and excited $S_1(\pi,\pi^*)$ electronic states. The DFT and ab initio calculations were very helpful for assigning the experimentally observed frequencies. The calculated values for

TABLE 3: SVLF Spectra (cm^{-1}) of 14DHN[a]

0_0^0		54_0^2		28_0^2		53_0^2		
0 vvs		+157 s		+184 m		+229 s		inferred[b]
−35 vvw	54_1^0 (B_2)	−35 vvw	54_1^2					
−71 m	54_2^0 (A_1)	−71 vvs	54_2^2					
		−112 s	54_3^2					
−148 w	28_1^0 (A_2)	−148 vs1	$28_1^0 54_0^2$					
		−157 m	54_4^2 (A_1)					
		−187 m	$28_1^0 54_1^2$ (B_1)	−183 vvw	$28_1^2 54_1^0$			−(148 + 35)
		−215 mw	$28_1^0 54_2^2$ (A_2)					−(148 + 71)
−231 vvw	53_1^0 (B_2)	−231 ms	$53_1^0 54_0^2$					
				−240 m				
		−268 mw	$53_1^0 54_1^2$ (A_1)			−268 vs	$53_1^2 54_1^0$	−(231 + 35)
−298 mw	28_2^0 (A_1)			−298 vvs	28_2^2			
						−315 m	?	
−346 w1	$53_0^0 54_3^0$ (A_1)					−341 ms	$53_1^2 54_3^0$	−(231 + 112)
−375 vvw	27_1^0 (A_2) ?	−375 w	$27_1^0 54_0^2$?	−374 ms	$27_1^0 28_0^2$?			
−453 m	18_1^0 (A_1)	−453 mw	$18_1^0 54_0^2$ (A_1)			−452 vvw	$18_1^0 53_0^2$	
		−466 mw	$53_2^0 54_0^2$ (A_1)			−465 w	53_2^2	2 × −(231)
−472 m	?							
−496 m	44_1^0 (B_1)							
−596 vs	17_1^0 (A_1)	−596 mw	$17_1^0 54_0^2$	−596 ms	$17_1^0 28_0^2$			
		−610 w	$18_0^0 54_4^2$ (A_1)					−(453 + 157)
−663 m	$17_1^0 54_2^0$ (A_1)	−664 s	$17_1^0 54_2^2$			−661 vw	$17_1^0 53_0^2 54_2^2$	−(596 + 71)
		−696 mw	$53_3^0 54_0^2$ (B_2)					3 × −(231)
		−707 mw	$17_1^0 54_3^2$					−(596 + 114)
−731 vvs	16_1^0 (A_1)	−732 m	$16_1^0 54_0^2$	−731 w	$16_1^0 28_0^2$	−732 vw	$16_1^0 53_0^2$	
		−738 m	$53_3^0 54_1^2$ (A_1)					−(698 + 35)
−750 mw	$18_1^0 28_0^2$ (A_1)	−752 vw	$18_1^0 28_0^2 54_0^2$	−753 w	$18_1^0 28_2^2$			−(453 + 29 8)
−772 m	$16_1^0 54_1^0$ (B_2)	−772 mw	$16_1^0 54_1^2$	−771 mw	$16_1^0 28_0^2 54_1^2$			−731 + 35)
−805 m	$16_1^0 54_2^0$ (A_1)	−806 vs	$16_1^0 54_2^2$					−(731 + 71)
−843 vvw	$16_1^0 54_3^0$ (B_2)	−845 s	$16_1^0 54_3^2$					−(731 + 112)
−855 m	?							
						−864 m	$17_1^0 53_1^2 54_1^0$ (A_1)	−(596 + 268)
−885 w	$16_1^0 54_4^0$ (A_1)	−885 vs	$16_1^0 54_4^2$					−(731 + 157)
−893 w	$17_1^0 28_2^0$ (A_1)			−894 vs	$17_1^0 28_2^2$			−(596 + 298)
−906 w	18_2^0 (A_1)							
−926 m	15_1^0 (A_1)							
		−971 mw	$18_2^0 54_2^2$ (A_1)					−(906 + 71)
						−1002 ms	$16_1^0 53_1^2 54_1^0$ (A_1)	−(731 + 268)
−1029 w	$16_1^0 28_0^2$ (A_1)			−1029 vs	$16_1^0 28_2^2$			−(731 + 298)
−1043 vs	14_1^0 (A_1)	−1043 mw	$14_1^0 54_0^2$	−1044 w	$14_1^0 28_0^2$	−1044 w	$14_1^0 53_0^2$	
−1077 w	$14_1^0 54_1^0$ (B_2)			−1077 m	$14_1^0 28_0^2 54_1^0$	−1077 m	$14_1^0 53_0^2 54_1^0$	−(1043 + 35)
−1115 m	$14_1^0 54_2^0$ (A_1)	−1116 vs	$14_1^0 54_2^2$					−(1043 + 71)
−1156 w	13_1^0 (A_1)	−1157 vs	$13_1^0 54_0^2$					
−1169 m	12_1^0 (A_1)	−1169 vvw						
−1190 s	11_1^0 (A_1)	−1193 vs	$11_1^0 54_0^2$					
−1200 mw	$14_1^0 54_3^0$ (B_2)							−(1043 + 157)
−1225 w	$11_1^0 54_1^0$ (B_2)							−(1190 + 35)
−1265 m	$11_1^0 54_2^0$ (A_1)	−1265 s	$11_1^0 54_2^2$					−(1190 + 71)
−1300 ms	10_1^0 (A_1)							
−1326 s	51_2^0 (A_1)							2 × −(661)
−1342 w	9_1^0 (A_1)							
−1460 vs	16_2^0 (A_1)							2 × −(731)
−1853 ms	15_2^0 (A_1)							2 × −(926)
−2084 vs	14_2^0 (A_1)							2 × −(1043)

[a] Key: s, strong; w, weak; m, medium; v, very. [b] Inferred from the already assigned fundamental values.

the excited state were especially helpful as they made it possible to assign many experimentally observed frequencies to the correct normal modes of this state. The frequencies of the ground state vibrational modes determined by infrared and Raman spectra agree very well with those observed by SVLF spectra. SVLF also determined the energies of many higher vibrational levels and also of levels arising from the combination of different modes. Many vibronic levels of the excited state also were determined by FES spectra together with UV. The present work provides a complete vibrational assignment of 14DHN molecule in both its electronic ground and singlet excited states for the first time.

TABLE 4: Some Selected UV Bands (in cm^{-1}) of 14DHN

UV	assignment	inferred[a]	
−153.2 vw	$53_1^0 54_0^1$	−153.6	77.4−231
−142.9 ms	$28_2^0 54_0^2$	−140.8	157.2−298
−114.3 ms	53_1^1	(−116)	[115]−231
−81.7 w	54_4^1	−82.7	77.4−160.1
−85.0 s	$28_0^2 53_0^1 54_0^1$	−85.8	182.2−268
−72.2 s	54_2^0		
−57.8 vs	$28_{01}^{0\ 1}$	(−56)	[92]−148
−36.5 m	$54_{03}^{0\ 1}$	−37.0	77.4−114.4
−19.2 m	$28_1^1 54_1^1$	(−17.6)	[169.4]−187
−4.1vvw	54_4^2	−2.9	157.2−160.1
6.4 w	$54_{02}^{0\ 1}$	5.2	77.472.2
8.2 w	$53_1^0 54_0^3$	7.4	238.4−231
23.9 ms	$28_2^0 54_0^4$	22.8	320.8−298
43.7 vs	54_1^1		
77.2 s	54_0^1		
85.0 vs	54_2^2		
111.6 w	$28_0^2 54_2^0$	110.0	182.2−72.2
124.1 s	54_3^3		
153.4 m	$53_0^2 54_2^0$	156.8	229−72.2
160.2 m	54_4^4	160.7	320.8−160.1
237.2 ms	54_0^3	238.4	

[a] Inferred from the energy level diagram shown in Figure 9.

Acknowledgment. The authors wish to thank the National Science Foundation (Grant CHE-0131935) and the Robert A. Welch Foundation (Grant A-0396) for financial support.

References and Notes

(1) Rishard, M. Z. M.; Wagner, M.; Yang, J.; Laane, J. *Chem. Phys. Lett.* **2007**, *442*, 182.
(2) Autrey, D.; Arp, Z.; Choo, J.; Laane, J. *J. Chem. Phys.* **2003**, *119*, 2557.
(3) Laane, J. *J. Phys. Chem. A* **2000**, *104*, 7715.
(4) Sakurai, S.; Meinander, N.; Morris, K.; Laane, J. *J. Am. Chem. Soc.* **1999**, *121*, 5056.
(5) Sakurai, S.; Bondoc, E.; Laane, J.; Morris, K.; Meinander, N.; Choo, J. *J. Am. Chem. Soc.* **2000**, *122*, 2628.
(6) Bondoc, E.; Sakurai, S.; Morris, K.; Chiang, W.-Y.; Laane, J. *J. Chem. Phys.* **2000**, *112*, 6700.
(7) Arp, Z.; Laane, J.; Sakamoto, A.; Tasumi, M. *J. Phys. Chem. A* **2002**, *106*, 3479.
(8) Arp, Z.; Meinander, N.; Choo, J.; Laane, J. *J. Chem. Phys.* **2002**, *116*, 6648.
(9) Yang, J.; Wagner, M.; Okuyama, K.; Arp, Z.; Choo, J.; Meinander, N.; Laane, J. *J. Chem. Phys.* **2006**, *125*, 034308.
(10) Yang, J.; Wagner, M.; Laane, J. *J. Phys. Chem. A* **2006**, *110*, 9805.
(11) Haller, K.; Chiang, W.-Y.; del Rosario, A.; Laane, J. *J. Mol. Struct.* **1996**, *379*, 19.
(12) Frisch, M. J.; Trucks, G. W.; Schlegel, H. B.; Scuseria, G. E.; Robb, M. A.; Cheeseman, J. R.; Montgomery, J. A., Jr.; Vreven, T.; Kudin, K. N.; Burant, J. C.; Millam, J. M.; Iyengar, S. S.; Tomasi, J.; Barone, V.; Mennucci, B.; Cossi, B. M.; Scalmani, G.; Rega, N.; Petersson, G. A.; Nakatsuji, H.; Hada, M.; Ehara, M.; Toyota, K.; Fukuda, R.; Hasegawa, J.; Ishida, M.; Nakajima, T.; Honda, Y.; Kitao, O.; Nakai, H.; Klene, M.; Li, X.; Knox, J. E.; Hratchian, H. P.; Cross, J. B.; Bakken, V.; Adamo, C.; Jaramillo, J.; Gomperts, R.; Stratmann, R. E.; Yazyev, O.; Austin, A. J.; Cammi, R.; Pomelli, C.; Ochterski, J. W.; Ayala, P. Y.; Morokuma, K.; Voth, G. A.; Salvador, P.; Dannenberg, J. J.; Zakrzewski, V. G.; Dapprich, S.; Daniels, A. D.; Strain, M. C.; Farkas, O.; Malick, D. K.; Rabuck, A. D.; Raghavachari, K.; Foresman, J. B.; Ortiz, J. V.; Cui, Q.; Baboul, A. G.; Clifford, S.; Cioslowski, J.; Stefanov, B. B.; Liu, G.; Liashenko, A.; Piskorz, P.; Komaromi, I.; Martin, R. L.; Fox, D. J.; Keith, T.; Al-Laham, M. A.; Peng, C. Y.; Nanayakkara, A.; Challacombe, M.; Gill, P. M. W.; Johnson, B.; Chen, W.; Wong, M. W.; Gonzalez, C.; Pople, J. A.; *GAUSSIAN 03, Revision C.02*; Gaussian, Inc.: Wallingford, CT, 2004.
(13) Yang, J.; McCann, K.; Laane, J. *J. Mol. Struct.* **2004**, *695−696*, 339.
(14) Autrey, D.; Haller, K.; Laane, J.; Mlynek, C.; Hopf, H. *J. Phys. Chem. A* **2004**, *108*, 403.
(15) Autrey, D.; Yang, J.; Laane, J.xy *J. Mol. Struct.* **2003**, *661−662*, 23.
(16) Al-Saadi, A. A.; Laane, J. *J. Mol. Struct.* **2007**, *830*, 46.
(17) Dennington, R., II; Keith, T.; Millam, J.; Eppinnett, K.; Hovell, W. L. Gilliland, R., *GaussView, Version 3.09*; Semichem, Inc.: Shawnee Mission, KS, 2003.
(18) Chakraborty, T.; Del Bene, J. E.; Lim, E. C. *J. Chem. Phys.* **1993**, *98*, 8.

JP902672X